Plant Physiology Preview. Published on August 10, 2018, as DOI:10.1104/pp.18.00664

**Short title:** Active vision cell for 3D Plant Reconstruction

# Plant Phenotyping: An Active Vision Cell for Three-Dimensional Plant Shoot Reconstruction

**Jonathon A. Gibbs [A *], Michael Pound [A], Andrew P. French [A], Darren M. Wells [B], Erik Murchie [B] and Tony Pridmore [A]**

[A] School of Computer Science, University of Nottingham, Jubilee Campus, Nottingham, NG8 1BB, UK.
[B] School of Biosciences, University of Nottingham, Sutton Bonington Campus, Sutton Bonington, Leicestershire, LE12 5RD, UK.

***Corresponding author**: Jonathon A. Gibbs (psxjg6@nottingham.ac.uk)

**One sentence summary**: A modelling approach is presented for 3D plant shoot reconstruction to aid plant phenotyping by producing a more accurate representation of different plant types

**Author contributions**: J.G. Designed and implemented the system, performed the experiments and wrote the article; M.P. Support with 3D reconstructions; A.F., D.W., E.M. Support with biological relevance and fit for purpose; T.P. Supervised the project

**Funding:** This work was funded by Engineering and Physical Sciences Research Council PhD Studentship Award 1499261 (to J.A.G.) and Biotechnology and Biological Sciences Research Council BBSRC Grant BB/R004633/1, "The 4-dimensional plant: enhanced mechanical canopy excitation for improved crop performance”.

**Keywords**: Reconstruction, phenotyping, active vision, plant

## ABSTRACT

Three-dimensional (3D) computer-generated models of plants are urgently needed to support both phenotyping and simulation-based studies such as photosynthesis modelling. However, the construction of accurate 3D plant models is challenging as plants are complex objects with an intricate leaf structure, often consisting of thin and highly reflective surfaces that vary in shape and size, forming dense, complex, crowded scenes. We address these issues within an image-based method by taking an active vision approach, one that investigates the scene to intelligently capture images, to image acquisition. Rather than use the same camera positions for all plants, our technique is to acquire the images needed to reconstruct the target plant, tuning camera placement to match the plant’s individual structure. Our method also combines volumetric- and surface-based reconstruction methods and determines the necessary images based on the analysis of voxel clusters. We describe a fully automatic plant modelling/phenotyping cell (or module) comprising a six-axis robot and a high-precision turntable. By using a standard colour camera, we overcome the difficulties associated with laser-based plant reconstruction methods. The 3D models produced are compared with those obtained from fixed cameras and evaluated by comparison with data obtained by X-ray μ-computed tomography across different plant structures. Our results show that our

method is successful in improving the accuracy and quality of data obtained from a variety of plant types.

## INTRODUCTION

With the population increasing and expected to reach 9 billion within the next four decades it is no wonder that demand for food is increasing (Sticklen 2007; Paproki et al. 2012; Faaij 2008). Moreover, developing countries, such as China and India, are increasing food intake per capita and driving the demand for a richer, more varied diet, such as meats and dairy. Climate change, leading to more frequent and severe flooding, and a shortage of arable land constitute additional challenges. Furthermore, it has been predicted that without crop climate adaptation the production of food will deteriorate (Challinor et al. 2014; Adeloye 2010). In order to deal with such demands, innovative approaches to increasing agricultural production are necessary.

Connections between the underlying genetic code and visible physical structures and functions of plants (i.e. phenotyping) can aid the identification of more productive crop species. A comprehensive understanding of plant phenotypes informs breeding and genetic selection, facilitating, for example, more effective nutrient use and photosynthetic activity, thereby increasing crop yield and stability across more extreme environments (Quan et al. 2006). The relationship between phenotype and genotype has received an increased amount of attention over recent years, with significant progress made in the study of genetics. The recovery and analysis of traits such as plant growth, development and tolerance, however, remains a serious bottleneck (Furbank., & Tester 2011). Two-dimensional (2D) approaches to plant phenotyping have been used extensively, though they have numerous limitations; most notably the inability to accurately reflect 3D quantities. For example, a curved leaf in a 2D image will have a significantly smaller surface area than in a 3D model. 2D methods struggle to capture plant structure and accurate measurement of growth is challenging. The use of 3D models overcomes many of these difficulties, allowing more and more traits to be accurately obtained. Once a 3D model of a given plant has been built it can be re-analysed, should new trait measurements be required. This may not be possible in 2D approaches, where image acquisition is often designed to provide a particular, limited, set of data. Access to accurate 3D models also supports simulation-based studies of plant functions, such as photosynthesis (Burgess et al. 2015; Burgess et al. 2017).

The construction of accurate 3D models of plants is extremely challenging. Existing approaches fall into the two categories of *rule-based* or *image-based* (Remondino & El-Hakim 2006). Rule-based approaches use knowledge of plant structure, forming and generating example models consistent with that knowledge. Though rule-based approaches can produce satisfactory results, their use often requires expert knowledge, and rules are usually targeted towards specific plant types. Plant structure also varies significantly across species and environments, making it difficult to predict structures *a priori*. More importantly, though they can generate visually realistic models, the representations produced may not correspond to any real, existing plant. Consequently, rule-based models are unsuitable for high resolution phenotyping tasks. In contrast, image-based methods develop accurate 3D models of real, viewed plants. These models can be used to support both simulations of plant function and the extraction of trait measurements (e.g. Burgess et al. 2015; Burgess et al. 2017).

One of the more popular approaches to 3D modelling is Multi-View Stereo (MVS). Here a number of images (several tens) are captured from distinct viewpoints. Given sufficient overlap between views, it is possible to match features between images and produce a 3D point cloud, to which a surface can be fitted. Though MVS has been successful in a variety of domains, plants are particularly challenging objects to model. Individual leaves can be very similar in appearance, and densely-packed; occluding each other from many viewpoints. They often lack the surface texture needed when matching image features, assuming local coherence and smoothness. The leaves of many species are also highly reflective, making alternative laser scanning approaches less effective. For a review of 3D modelling algorithms for plants readers are encouraged to see (Gibbs et al. 2017).

The high-throughput phenotyping systems deployed in plant and crop science are now routinely gathering large numbers of images from which 3D models might be obtained. Current installations, however, typically rely on fixed viewpoints that are not adapted to the specific plant being examined, or are designed with one species in mind. Some systems rotate the plant during imaging, but still use static camera positions. The relation between viewpoints and plant therefore remains fixed, regardless of the structure of the plant, which may vary widely. This means that, in many cases, the images captured are far from optimal for the given plant. In order to capture 3D models useful for phenotyping, there is a need for a more intelligent image capture system optimised for 3D reconstruction, and sensitive to variations in plant architecture.

In this work we show that active computer vision (Aloimonos et al. 1988) can aid the reconstruction of complex plants by providing reactive, and therefore improved, image acquisition strategies. Active vision systems automatically control and manipulate camera viewpoints to gather information to best support the task at hand. Active vision methods have already played a role in other plant-related tasks. For example, Hemming et al. (2014) attach a camera to a robot arm in order to identify peppers to be collected. The effect of camera placement on fruit picking has also been investigated (Hemming et al. 2014), with active vision used to address the problem of occlusion. The process of capturing images for 3D reconstruction, known as image selection, is, however, currently an insufficiently considered resource in image-based 3D reconstruction (Hornung 2008).

We propose a framework to automatically capture a set of images suitable for use in 3D modelling, via MVS, of different and contrasting plant structures. This work directly addresses the competing demands placed on image acquisition; too large a set of images can introduce redundancy and results in excessive processing times, whilst too few images results in an incomplete model. We identify a set of viewpoints that enable a reliable 3D model to be reconstructed without excessively scanning the plant. We present a solution suitable for deployment in an automated, high-throughput phenotyping system. The present paper describes a fully automated, active vision cell (AVC) that is capable of manipulating a camera's viewpoint to produce high quality 3D models of a wide range of plants by adapting to the visual information available, without user intervention. The approach described here offers more flexibility than existing large-scale phenotyping systems by adapting to the natural variation of individual plants. This is achieved by investigating an initial, crude representation of plant structure in order to re-position the camera and obtain improved data.

## SET UP/ METHOD DEVELOPMENT

The accuracy and reliability of 3D models depends heavily on the *quality* of images, whilst its computational requirements are dependent on the *number* of images. Images do not contribute equally to the quality of a reconstruction; some are redundant while others add large amounts of high quality, necessary data (Seitz et al. 2006). Here, we propose an AVC designed to provide sufficient data to ensure a reliable representation without the need for specific expertise on the part of the user and with the ability to adapt to different plant structures, and without analysing excess numbers of images.

### *Cell Design and Calibration*

Our AVC is comprised of three main components: a high precision turntable (**LT360EX** – Linear X Systems, Portland, USA) with a resolution of 0.0015 degrees, a robot arm providing 6 degrees of freedom (**UR5** – Universal Robots, Odense, Denmark) and a standard colour camera (**Canon 650D** – Canon, Tokyo, Japan) mounted on the robot arm (Figure 1). A single software interface is used to control each of the hardware components. The UR5 is sent commands using strings via sockets, the LT360EX is controlled using serial communications and the Canon 650D via an Software Development Kit (SDK).

Calibration, the process of obtaining reliable 3D camera parameters for each view, is an important first-step in any 3D reconstruction pipeline. Calibration is usually an automatic process, determining the physical parameters of each hardware component, and quantifying the relationships between them and the viewed environment. The calibration process can be organised into four stages; camera calibration, robot calibration, calibration of the remaining unknowns and turntable calibration. All four calibration steps are required to determine the position of the camera for active vision. In simple terms, the calibration aims to estimate the position and orientation of each component in the setup (the robot and turntable), and the camera lens and sensor.

**Camera Calibration** is used to estimate the intrinsic and extrinsic parameters of the camera which are used to determine its location for the calibration of the robot. A standard checkerboard calibration target, in which the dimensions of the squares are known, is placed on the turntable. Given a series of images of this calibration object at distinct viewpoints, it is possible to recover the position, orientation and internal parameters of the camera that captured each image. Internal parameters are often termed intrinsic parameters, and consist of the focal length, offset and axis skew (Zhang 2000). The 3D plant models produced are expressed in *world coordinates* – with respect to a coordinate frame located on the checkerboard. The bottom right corner of the checkerboard is the world origin (0, 0, 0). *Camera calibration* provides a transformation between world coordinates and a coordinate frame centred on the camera. This transformation can be used to project any 3D world position into a 2D camera position in its image frame.

**Robot calibration** estimates the position and orientation of the end of the robot arm (i.e. the end effector). Also known as forward kinematics, robot calibration is achieved using a simultaneous closed-form quaternion approach (Dornaika & Horaud 1998). This produces a transformation matrix specifying the relationship between the base of the robot and the end effector. This transformation matrix provides the rotation and translation needed to transform one robot position to another.

**Calibration of unknowns**. After transformations linking the base of the robot to the camera, and the camera to the world (turntable) are available, it is possible to calculate the relationship between the base of the robot and the turntable (world). The remaining calibrations can be calculated as linear equation in the form of AX=YB, where A [the world to camera] and B [the robot base to the end effector] are now known and where Y [the world to robot base] and X [the camera to the end effector] are the two unknowns. A closed form approach to the linear equation has been used to determine the remaining unknowns (Dornaika & Horaud 1998).

**Turntable calibration**. Rotating the turntable, which is necessary to provide complete access to the plant, changes the relationship between robot/camera and world-coordinates. To calibrate the turntable, it is rotated by 90° four times. The camera is re-calibrated each time, giving four positions for the world coordinate origin. Plotting the four origins obtained from the calibration in two dimensions and connecting the diagonal origins using a straight line allows the centre of rotation to be solved as a line intersection problem. The centre of rotation is used to calculate a new world-coordinate frame each time the turntable is rotated. At this point, we have a fully parameterised relationship between the camera system, robotic arm and the turntable.

***Active Image Acquisition***

There are two stages to 3D modelling within the AVC; the first requires the creation of a crude, initial plant model, represented by a series of voxels, the second stage involves an analysis of this initial representation to identify under- and over-sampled (imaged) regions of the plant. The robot arm is then automatically directed to acquire more data, while unnecessary images are removed. Note that the images used to construct the volumetric proxy are also determined automatically, on the basis of 2D image features, as described below.

*An Initial Volumetric Plant Representation*

To acquire an initial volumetric representation of a plant we capture a series of images. These are taken from automatically determined camera locations circling the plant at three different heights. The first image is acquired after positioning the camera so that its principle axis (line of sight) lies in the plane of the turntable and passes through its centre of rotation. A Euclidean colour filter, which filters pixels where the colour is inside or outside of an Red, Green and Blue (RGB) sphere with a specified centre and radius, is applied to separate plant pixels from the white background. We then apply three simple rules to move the camera to centre the plant (which may be of arbitrary size, asymmetric, etc.) within the camera's field of view (FOV); these are: **1.** if there is too much white space surrounding the plant region (i.e. if the distance from the plant region to the edge of the image is greater than a specified threshold), move the camera forwards. **2.** If one side of the plant is outside the camera's FOV, move laterally to ensure it is inside, **3**. If more than one side is outside the camera's FOV, move the camera backwards. The resulting camera location forms the starting point for image acquisition. Once an acceptable viewpoint has been determined a series of images is captured by rotating the plant and acquiring an image every 36 degrees, producing 10 images with the camera fixed at the initial elevation.

Space carving (Seitz 2000) is used to generate the initial 3D model from the first image sequence. Space carving operates by projecting the silhouette of the target object (the plant) into 3D space to define the volume possibly occupied by the object. Projecting silhouettes extracted from multiple images, and taking the intersection of the volumes they produce, reduces the size of this volume, creating an increasingly more accurate model.

This 10-image model of a complex plant (Figure 2) is of limited value, but does allow an estimate of the plant height to be made. The camera is raised to be level with the top of the plant, automatically re-centred as described above, and a further 10 images are acquired by rotating the turntable. This is known as the level 2 position, having moved up along the z-axis in one increment, where the first set of images were captured at level 1, in line with the turntable. To improve coverage, the turntable is rotated 12 degrees before image acquisition begins. This means that the level 1 and 2 camera positions are not aligned vertically but offset by 12 degrees. The new images are then used to refine the volumetric model, and therefore, plant height estimation.

To complete the volumetric representation, the camera is raised to twice the newly estimated height of the plant, a further 12 degrees offset is added and a final 10 images acquired. By increasing the height of the camera to above the height of the plant, it is possible to get a set of top down images uncovering new information, particularly useful for plants with wide flat leaves, such as broadleaf species including legumes and squashes.

This image acquisition strategy is designed to achieve a set of varying viewpoints that sample the area around the plant while keeping the plant in view. Note that we do not re-centre the plant in each image, only the first captured at each level. However, given plants with a high degree of asymmetry the rules above could be applied after each rotation of the turntable.

The final volumetric model remains comparatively crude and low resolution, giving a ‘blocky’ appearance, and is unable to represent some features at all, such as concavities. It does however provide a sufficient intermediate representation for evaluation via forward ray tracing (Vasquez-Gomez et al. 2013), in which rays from the camera are projected into the scene to determine intersection with the object, and so determines which cameras can see what parts of the developing 3D model.

*Plant Model Refinement*

The next step is the automatic refinement of the image set, removing those that are unnecessary, and obtaining further images of under-represented sections of the plant. Images are removed if each voxel in the plant proxy representation is still seen by more than 3 cameras after their removal. In practice MVS produces higher quality results when an area has been seen 3 times or more.

View planning is then performed to determine which additional data to capture. Traditionally, view planning evaluates each possible view on a per voxel basis; each voxel is evaluated independently for every possible camera position in the view sphere (Massios & Fisher. 1998; Wong et al. 1999). If we were to do this in our cell, and if we limit robot movements in whole degrees, it is possible to move 180 points from top to bottom and 360 points around the view sphere, resulting in 64,800 camera positions that would require evaluation. We reduce this complexity by clustering voxels together and evaluating specific views on a per-cluster basis. There are four stages here: 1. Clustering, 2. Cluster evaluation, 3. Camera placement and 4. Data acquisition.

**1. Clustering.** Each voxel is represented by a single point lying at its centre, and the K-nearest neighbour (k-NN) algorithm is used to cluster the point set. k-NN is a simple machine learning algorithm that clusters the point set into a series of *k* nearest neighbours. That is, points are added to some cluster which are within the range of the centroid when given some radius. K-NN finds the k nearest neighbours to a point which are within some radius of the centre of the cluster, the starting point. We implement this algorithm using a KD-tree data structure, which significantly improves performance when applying nearest-neighbour searchers to points in K dimensions.

**2. Cluster evaluation**. Each cluster must be evaluated to determine whether additional images need to be captured and thus to ensure that the object is sufficiently scanned. We propose a simple evaluation method that operates on the number of views in which a cluster is visible, and the angle between the cameras which have seen the cluster (Furukawa & Ponce 2010). If a cluster has a low score then we mark the cluster as requiring additional viewpoints. The evaluation metric used is given in (Eq. 1):

$$Score = \frac{1}{C_n}\sum_{j=1}^{C_n}\left(\frac{seen(C_j)}{imgCrit} + \frac{maxAngle(C_{cam}, C_{cam})}{angleCrit}\right) \times 0.5$$

*(Eq. 1)*

where $\boldsymbol{seen(C_j)}$ refers to the number of times each voxel has been seen in the cluster and $\boldsymbol{imgCrit}$ is the number of times a point must be seen to ensure an accurate representation (we use 3 to match our PMVS settings). $\boldsymbol{maxAngle(C_{cam}, C_{cam})}$ is the maximum angle between any of the cameras that can see the voxel, and $\boldsymbol{angleCrit}$ is the minimal angle difference between cameras, to ensure different views (we use 20 degrees, determined empirically).

We determine whether a cluster has been seen by a given camera via ray tracing. This simulates projection of a ray of light from the camera to the cluster centroid. In order to improve performance, we implement a Hierarchical Ray Tracing (HRT) (Vasquez-Gomez et al. 2013) approach rather than a Uniform Ray Tracing (URT) method. URT traces dense rays through the scene irrespective of whether an intersection with a voxel occurs. HRT traces sparse rays, only increasing the resolution when voxels are touched by a ray. Starting at a coarse resolution HRT continues until the maximum resolution is reached.

**3. Camera placement.** Given a series of under sampled clusters we proceed to calculate a series of viewpoints that can be used to capture additional information. We first determine the distance the camera is required to be from the object, to ensure the plant is completely within the field of view, without excess white space, using the camera parameters and object size. The size of our view sphere (**Error! Reference source not found.**) is then determined by (Eq. 2):

$$FOV = 2 \cdot atan(\frac{1}{2} \cdot \frac{s}{f})$$

$$Distance = \frac{1}{2} \cdot \frac{\max(w, h)}{\sin(\text{FOV})}$$

*(Eq. 2)*

where $s$ is the sensor size, $f$ is the focal length, both of which are obtainable from the camera specification. $max(w, h)$ returns the maximum value of the object with respect to the height, $h$, and width, $w$.

Traditional view-planning methods evaluate every possible position on the view sphere; we significantly reduce the heavy computational requirements this brings by incrementally expanding our search should a view fail. A starting camera position is defined as the intersection of the normal of the cluster with the view sphere. The view is evaluated for correctness in two ways, the first is to perform inverse kinematics to ensure that the robot is able to reach the position, the second is ray tracing from the camera position into the scene to ensure the cluster is not occluded from this viewpoint. If either of the evaluations fail we incrementally expand over the view sphere, first evaluating positions in green (Figure 3) and then yellow, and so on, expanding outwards from the starting position until an acceptable viewpoint is found. This process is performed for each cluster that requires additional viewpoints to be captured, until views of all clusters have been obtained.

**4. Data acquisition.** Once we have a series of camera positions, additional images are captured as necessary, and PMVS (Furukawa & Ponce 2010) is used to generate a point cloud that can support surface reconstruction.

## EVALUATION AND DISCUSSION

### *Active Cell Evaluation*

Having a more accurate set of points that closely represent the surface of some unknown object significantly improves the quality of any subsequent 3D model as they more faithfully represent the actual shape of the object. Moreover, a larger number of points further facilitates the faithful reconstruction by providing more detail of the plant structure.

*Ground truth model*

In order to evaluate our AVC's point clouds, X-ray images of our target plants were obtained using a GE v|tome|x M scanner housed in the University of Nottingham's Hounsfield Facility. The v|tome|x M provides volumetric images with a voxel resolution of 5 - 150 µm and, more importantly, is not subject to the occlusion problems faced by visible light imaging. Though some X-ray segmentation tasks are highly challenging, plant material and air are easily separated in the density data provided by µCT and, following noise reduction with a median filter, plant material was identified by applying a user-defined threshold. A complete image of the plant is formed. The surface of each plant was then represented in a standard triangular mesh format, providing a data structure (i.e. a ground truth model) against which point clouds obtained from the AVC can be compared.

It is worth noting that while the µCT scanner produces accurate, highly detailed models, it is ill suited for general use in phenotyping shoots due to size restrictions, time requirements (typically taking hours to scan a single object, in comparison to minutes taken by the method here) and the exceptionally high start-up costs. Moreover, thin structural areas of the plant can still be missed, resulting in an incomplete reconstruction. However, it is useful for creating 3D ground truth models with which to compare a visual imaging system, as occlusion is not a problem for x-ray µCT.

*Comparative image-based models*

The AVC-derived model was compared to traditional static and arbitrary camera placements. Static setups use one or more cameras that remain fixed in place, irrespective of the plant being modelled. Typically, the plant is rotated and images are captured. In the experiments conducted in this work the method '*one static*' refers to the use of a single static camera placed horizontally alongside the plant, such that the whole plant is visible in the camera's field of view. '*Two static*' uses two fixed cameras, using the same placement as *one static* and adding a further camera placed higher, vertically, above the other such that a top down view of the plant is obtained. '*Arbitrary*' refers to the process of capturing images of the plant at distinct random positions and is commonly the method used when users manually capture images of plants.

Two evaluation metrics were employed; number of points obtained and the distance from those points to the surface of the x-ray µCT ground truth. Euclidean distance was used to determine the error of a point in the gathered data with respect to the surface of the ground truth. Six experiments were performed on plants varying in size, structure and complexity, namely; Bromeliad (*Vriesea* sp.), Aloe (*Aloe vera*), Cordyline (*Cordyline* sp.), Brassica (*Brassica napus*), chilli (*Capsicum* sp.) and pumpkin (*Cucurbita pepo*). The method is not limited to these plants and can be applied to plants which are much larger such as wheat (*Triticum* sp.), maize (*Zea mays*) and barley (*Hordeum vulgare*), or other important crop species, with the only size restrictions relating to the reach of the robot arm.

### *Experiment One*

Experiment one was conducted on a bromeliad (*Vriesea* sp. Figure 4). The *Bromeliaceae* are a family of monocot flowering plants in which over 3,400 species are known, native to the tropical Americas. While foliage takes different shapes and forms the one used in this experiment is thin, broad and flat. Consequently, views from above the plant, clearly seeing the wide leaves, will offer a great amount of insight into the plant size and structure. Occlusion however makes this problematic for static cameras that may be unable to see underlying leaf surfaces.

| | Mean | Std.Dev | Points | Images | Per Image |
|---|---|---|---|---|---|
| One Static | 0.3574 | 1.1795 | 141,073 | 40 | 3,526.80 |
| Two Static | 0.3442 | 0.7450 | 155,396 | 40 | 3,884.90 |
| Arbitrary | 0.2693 | 1.1267 | 227,338 | 40 | 5,683.50 |
| AVC | 0.1959 | 0.6773 | 290,236 | 36 | 7,637.80 |

**Table 1** Experiment One Results - bromeliad

Table 1 compares the AVC approach to a static camera configuration. *Mean* refers to the distance of the points relative to the ground truth model; *Std.Dev* to error of that distance; *Points* to the number of points representing the 3D model and the number of points generated *per image* captured. When using a point cloud to drive a surface reconstruction approach (e.g. Pound et al. 2014) higher numbers of points allow a finer granularity on reconstructed surface patches, and higher number of points per image indicate that more data can be generated for each image captured. Lower mean and std. dev errors also impact the quality of the surface reconstruction; where lower values illustrate a more accurate representation when compared to the ground truth. For the Bromeliad, the AVC cell proposed here significantly out performs the two static methods obtaining more than 115% points in the first case, primarily due to the structure of the leaves, making it challenging for static cameras to view the leaf surface. In comparison to the arbitrary viewpoints we see that we can increase the points per image by almost 35% showing that intelligently selecting viewpoints in AVC improves performance despite fewer images, that is we are obtaining more data per image. Furthermore, the reduction in the mean value by 27% shows that a more accurate point cloud is being produced (Supplementary Figure S1).

***Experiment Two***

Experiment two was conducted on *Aloe vera* (Figure 5). The upwards leaves occlude plant structure that lie directly behind them making it challenging for views that are side on. Like the bromeliad from experiment one it consists of flat wide surfaces with little texture. Table 2 illustrates the results of the four image acquisition methods.

| | Mean | Std.Dev | Points | Images | Per Image |
|---|---|---|---|---|---|
| One Static | 1.4517 | 3.6624 | 159,870 | 40 | 3,996.80 |
| Two Static | 1.6911 | 3.6143 | 160,592 | 40 | 4,014.80 |
| Arbitrary | 1.8963 | 4.5674 | 183,027 | 40 | 4,575.70 |
| AVC | 1.3329 | 3.5930 | 216,791 | 31 | 5,705.00 |

**Table 2** Experiment Two Results – aloe Vera

From Table 2, we see our AVC here outperforms each of the standard methods obtaining at least 18% more points while using 22.5% less images. One static view obtains the least amount of points, unable to deal with the concavities caused by the wide upright leaves.  Two static also has less points, despite having two views it is unable to obtain the data occluded by the outer leaves. Arbitrary viewpoints do overcome some of the occlusions but does not capture enough to deal with it completely. The AVC deals with the occlusions and recovers more accurate points with a reduced image set.

### *Experiment Three*

Experiment three uses a Cordyline (*Cordyline* sp.), a genus of approximately 15 species of monocotyledonous flowering plants in the family *Asparagaceae* (Figure 6). Unlike the previous two experiments, experiment three focuses on a thin upright plant which is particularly crowded and occluded towards the base but relatively sparse towards the tips of the stems.

| | Mean | Std.Dev | Points | Images | Per Image |
|---|---|---|---|---|---|
| One Static | 0.7565 | 2.0167 | 122,851 | 40 | 3,071.30 |
| Two Static | 0.8638 | 2.8122 | 94,193 | 40 | 2,354.80 |
| Arbitrary | 1.0284 | 4.7614 | 80,154 | 40 | 2,003.90 |
| AVC | 0.7384 | 2.0691 | 143,049 | 26 | 3,764.40 |

**Table 3** Experiment Three Results - *Cordyline*

From Table 3, we see our AVC significantly out performs the *arbitrary* and *two static* view, but unlike the previous experiments, it has a smaller improvement over the traditional *one static* view. This highlights the fact that randomly adding images does not necessarily lead to an improvement and, in some cases, additional noise is added. As the plant contains few occlusions and has very thin non-drooping leaves it is possible to capture a significant amount of information from a side view. However, despite the similarity of results between *one static* and our AVC points, our AVC uses 35% less images (26 relative to 40) than the single camera and obtains, on average, 22% more data per image used. This again shows that manipulating the viewpoint can improve accessibility to data and thus optimises the processing power and time required to create a 3D model.

### *Experiment Four*

Experiment four was conducted on a Brassica (*Brassica napus*), an agriculturally important member of the *Brassicaceae* family (Figure 7). This is a very small plant and, to avoid missing plant data, views need to be taken much closer than the previous experiments. A traditional static image acquisition strategy may struggle if not specifically designed for small plant species as the camera will be positioned much further away from the plant than necessary.

| | Mean | Std.Dev | Points | Images | Per Image |
|---|---|---|---|---|---|
| One Static | 0.2007 | 0.7208 | 97,191 | 40 | 2,429.8 |
| Two Static | 0.0867 | 0.4427 | 146,743 | 40 | 3,668.6 |
| Arbitrary | 0.1682 | 0.5466 | 178,418 | 40 | 4,460.5 |
| AVC | 0.0354 | 0.3912 | 349,311 | 21 | 16,633.9 |

**Table 4** Experiment Four Results - Brassica

Table 4 indicates that the AVC captures more data despite using only half the images. This confirms that images in MVS reconstruction do not contribute evenly to the success of a reconstruction, but rather it is the quality of the images that has the greatest effect on the results.

### *Experiment Five*

Experiment five was conducted using a chilli (*Capsicum* sp.) which are widely grown in many countries as a cash crop (Figure 8). Similar to experiment four, the plant used was at an early developmental stage and thus is of small size. Static cameras may miss data particularly as the leaves and stems are thin.

| | Mean | Std.Dev | Points | Images | Per Image |
|---|---|---|---|---|---|
| One Static | 0.2380 | 0.9420 | 113,284 | 40 | 2,832.1 |
| Two Static | 0.1843 | 0.4245 | 247,442 | 40 | 6,186.1 |
| Arbitrary | 0.2536 | 2.2226 | 199,023 | 40 | 4,975.6 |
| AVC | 0.1022 | 0.4584 | 285,381 | 28 | 10,192.2 |

**Table 5** Experiment Five Results - Chilli

Table 5 indicates again that the AVC is capable of capturing more, and, importantly, more accurate, data points from fewer images when compared with traditional methods. Though the two static camera approach does have a lower standard deviation, it achieves this with many additional images.

***Experiment Six***

Experiment six was conducted using a pumpkin (*Cucurbita pepo*; Figure 9). The large flat leaves make occlusions for data acquisition a major problem, with the leaves often blocking the stem. Moreover, flat surfaces of plants are often problematic to reconstruct due to a lack of texture. Table 6 shows the results of the 4 approaches to image acquisition.

| | Mean | Std.Dev | Points | Images | Per Image |
|---|---|---|---|---|---|
| One Static | 1.1220 | 1.8674 | 715,222 | 40 | 17,880.6 |
| Two Static | 1.2104 | 3.4723 | 517,039 | 40 | 12,926.0 |
| Arbitrary | 0.6982 | 1.8200 | 852,426 | 40 | 21,310.7 |
| AVC | 0.3588 | 1.3823 | 1,048,576 | 30 | 34,952.5 |

**Table 6** Experiment Six Results - Pumpkin

The large surface area results in the high number of points produced for this model (Table 6). As a result of the large surface area, with minimal texture, the standard deviation for all methods is greater than for previous experiments (above). This is due to the difficulties associated with feature matching in PMVS. Despite this, the AVC is still able to produce an improved set of images with a smaller mean and larger set of points per image than any of the other methods.

*Biological Application of the AVC approach*

Methods for the accurate 3D representations of plants (that are also accessible to many research groups) are increasingly important to basic and applied research; for making new discoveries about plant function in addition to providing new traits for crop improvement. We still do not have a full understanding about how molecular and leaf level events are scaled to the whole plant and field level and how this limits productivity. For example, there is a disconnect between phenotypes in growth rooms and those in more challenging field environments (Poorter et al. 2016). Nor is there a complete understanding of the 'canopy factors' that cause variation in radiation use efficiency (Reynolds et al. 2000). The display of leaves to the sun and the way in which they influence the level of saturation of photosynthesis at each level is of huge importance to crop yield and optimising architecture (e.g by combining leaf angle traits with leaf density and possibly movement) (Burgess et al. 2015; Burgess et al. 2017; Long et al. 2006). Rapid and accurate means to achieve high resolution 3D reconstructions, such as the AVC described here, combined with more accurate ray tracing and physiological models, will enable us to do that.

The approach described here requires minimal user input; can be applied to any plant type or structure, with the only limitation on size being the reach of the robot arm. It is more accurate and requires less images than previous, static imaging approaches (Tables 1-6) and offers more flexibility than existing large-scale phenotyping systems by adapting to the natural variation of individual plants. The method is automatic with user input limited to changing the plant and is relatively quick with image capture and analysis relative to other methods, taking minutes as opposed to hours. Moreover, the method has reduced set up and running costs compared to some phenotyping systems such as x-ray µCT scanning.

## CONCLUSION

We proposed an active vision cell (AVC) for automatically capturing colour images of plants in a controlled environment, with a view to using them for 3D model reconstruction from multiple views. We have evaluated our method on varying plant structures and compared it to more traditional methods using arbitrary camera positions and static cameras, in terms of the number of points obtained and the accuracy of these with respect to the Euclidean distance to the ground truth.

In all experiments our AVC produces more data of higher accuracy, with a reduced image set. More points help ensure that the plant has been adequately scanned and that the amount of unknown object data is minimal. More accurate points ensure that the 3D model can be reconstructed with increased fidelity which is vital for accurate plant phenotyping. The AVC acquires more points per image indicating that the images captured provide more value towards reconstruction. While static camera placement can be effective, there are clear data gains to be made by employing active vision.

## Supplemental Data

**Supplemental Figure S1.** 3D reconstructions generated by the comparable imaging methods.

**Supplemental Figure S1:** Row one; experiment one and two, row two; experiment three and four, row three; experiment five and six. The supplementary figure illustrates the 3D reconstructions generated by the comparable imaging methods. The 3D points shown here highlight the lack of accuracy and detailed when compared to the AVC method proposed here.

## FIGURE LEGENDS

**Figure 1** The Active Vision Cell comprised of a Canon 650D camera, a Universal Robot 5, and an LT360EX turntable upon which the plant is placed

**Figure 2** Initial representation; left an original image of a target plant (Bromeliad- *Vriesea* sp.), middle the initial representation after 10 images, right the final voxel model showing more object features after acquiring additional viewpoints

**Figure 3** The view sphere representation which encloses the plant being modelled such that it is centred. The Red dot is an example of an initial optimal viewpoint, should this fail it is expanded to green, then to yellow and so on.

**Figure 4** Experiment one conducted on a bromeliad (*Vriesea* sp.). The first column is the X-Ray data, obtained using a CT scanner, the top row presents a side view and the bottom row a top down view. The second column is a point set obtained using the AVC proposed here.

**Figure 5** Experiment two conducted on *Aloe vera*. The first column is the X-Ray data, obtained using a CT scanner, the top row presents a side view and the bottom row a top down view. The second column is a point set obtained using the proposed AVC.

**Figure 6** Experiment three conducted on a Cordyline (*Cordyline* sp.). The first column is the X-Ray data, obtained using a CT scanner, the top row presents a side view and the bottom row a top down view. The second column is a point set obtained using the AVC proposed here.

**Figure 7** Experiment four conducted on *Brassica napus*. The first column is the X-Ray data, obtained using a CT scanner, the top row presents a side view and the bottom row a top down view. The second column is a point set obtained using the AVC proposed here.

**Figure 8** Experiment five conducted on a chilli plant (*Capsicum* sp.). The first column is the X-Ray data, obtained using a CT scanner, the top row presents a side view and the bottom row a top down view. The second column is a point set obtained using the AVC proposed here.

**Figure 9** Experiment six conducted on the Pumpkin (*Cucurbita pepo*). The first column is the X-Ray data, obtained using a CT scanner, the top row presents a side view and the bottom row a top down view. The second column is a point set obtained using the AVC proposed here.

**BIBLIOGRAPHY**

Adeloye, A., 2010. Global Warming Impact: Flood Events, Wet-Dry Conditions and Changing Scene in World Food Security. *Journal of Agricultural Research and Development*, 9(1). Available at: http://www.ajol.info/index.php/jard/article/view/56128 [Accessed January 8, 2015].

Aloimonos, J., Weiss, I. & Bandyopadhyay, A., 1988. Active vision. *International Journal of Computer Vision*, 1(4), pp.333–356. Available at: http://www.scopus.com/inward/record.url?eid=2-s2.0-34250088854&partnerID=tZOtx3y1 [Accessed February 26, 2015].

Burgess, A.J. et al., 2017. Exploring Relationships between Canopy Architecture, Light Distribution, and Photosynthesis in Contrasting Rice Genotypes Using 3D Canopy Reconstruction. *Frontiers in Plant Science*, 8, p.734. Available at: http://journal.frontiersin.org/article/10.3389/fpls.2017.00734/full [Accessed July 26, 2018].

Burgess, A.J. et al., 2015. High-Resolution Three-Dimensional Structural Data Quantify the Impact of Photoinhibition on Long-Term Carbon Gain in Wheat Canopies in the Field. *Plant Physiology*, 169(2), pp.1192–1204. Available at: http://www.ncbi.nlm.nih.gov/pubmed/26282240 [Accessed June 1, 2017].

Burgess, A.J. et al., 2016. The 4-Dimensional Plant: Effects of Wind-Induced Canopy Movement on Light Fluctuations and Photosynthesis. *Frontiers in plant science*, 7, p.1392. Available at: http://www.ncbi.nlm.nih.gov/pubmed/27708654 [Accessed April 9, 2018].

Challinor, A. et al., 2014. A meta-analysis of crop yield under climate change and adaptation. *Nature Climate Change*. Available at: http://eprints.whiterose.ac.uk/78340/13/Challinor-etal-AR5-RevisionsFinal_with_coversheet.pdf [Accessed December 12, 2014].

Dornaika, F. & Horaud, R., 1998. Simultaneous robot-world and hand-eye calibration. *IEEE Transactions on Robotics and Automation*, 14(4), pp.617–622. Available at: http://ieeexplore.ieee.org/lpdocs/epic03/wrapper.htm?arnumber=704233 [Accessed November 27, 2014].

Faaij, A., 2008. *Bioenergy and global food security*, Available at: http://www.wbgu.de/fileadmin/templates/dateien/veroeffentlichungen/hauptgutachten/jg2008/wbgu_jg2008_ex03.pdf [Accessed November 24, 2014].

Furbank, R. T., & Tester, M., 2011. Phenomics – technologies to relieve the phenotyping bottleneck. *Trends in plant science*, 16(12), pp.635–644. Available at: https://www.plantphenomics.org.au/publications/2011TrendsFurbankTester.pdf [Accessed November 1, 2014].

Furukawa, Y. & Ponce, J., 2010. Accurate, dense, and robust multiview stereopsis. *IEEE transactions on pattern analysis and machine intelligence*, 32(8), pp.1362–76. Available at: http://www.ncbi.nlm.nih.gov/pubmed/20558871.

Gibbs, J.A. et al., 2017. Approaches to three-dimensional reconstruction of plant shoot topology and geometry. *Functional Plant Biology*, 44(1), p.62. Available at: http://www.publish.csiro.au/?paper=FP16167 [Accessed November 6, 2017].

Hemming, J. et al., 2014. A robot for harvesting sweet-pepper in greenhouses. In *Proceedings of the International Conference of Agricultural Engineering*. Available at: http://edepot.wur.nl/309949 [Accessed June 16, 2015].

Hemming, J. et al., 2014. Fruit detectability analysis for different camera positions in sweet-pepper. *Sensors (Basel, Switzerland)*, 14(4), pp.6032–44. Available at: http://www.mdpi.com/1424-8220/14/4/6032/htm [Accessed June 17, 2015].

Hornung, A., Zeng, B., & Kobbelt, L. (2008, June). Image selection for improved multi-view stereo. In *Computer Vision and Pattern Recognition, 2008. CVPR 2008. IEEE Conference on* (pp. 1-8). IEEE.

Long, S.P. et al., 2006. Can improvement in photosynthesis increase crop yields? *Plant, cell & environment*, 29(3), pp.315–30. Available at: http://www.ncbi.nlm.nih.gov/pubmed/17080588 [Accessed April 9, 2018].

Massios, Nikolaos A., and R.B.F., 1998. A best next view selection algorithm incorporating a quality criterion. *BMVC*.

Paproki, A. et al., 2012. A novel mesh processing based technique for 3D plant analysis. *BMC plant biology*, 12(1), pp.1–13.

Poorter, H. et al., 2016. Pampered inside, pestered outside? Differences and similarities between plants growing in controlled conditions and in the field. *New Phytologist*, 212(4), pp.838–855. Available at: http://www.ncbi.nlm.nih.gov/pubmed/27783423 [Accessed April 9, 2018].

Pound, M.P. et al., 2014. Automated recovery of three-dimensional models of plant shoots from multiple color images. *Plant physiology*, 166(4), pp.1688–98. Available at: http://www.plantphysiol.org/content/166/4/1688 [Accessed December 11, 2014].

Quan, L. et al., 2006. Image-based plant modeling. *ACM Transactions on Graphics*, 25(3), p.599. Available at: http://dl.acm.org/citation.cfm?id=1141911.1141929 [Accessed November 5, 2014].

Remondino, F. & El-Hakim, S., 2006. Image-based 3D Modelling: A Review. *The Photogrammetric Record*, 21(115), pp.269–291. Available at: http://doi.wiley.com/10.1111/j.1477-9730.2006.00383.x [Accessed January 8, 2015].

Reynolds, M.P., van Ginkel, M. & Ribaut, J.M., 2000. Avenues for genetic modification of radiation use efficiency in wheat. *Journal of experimental botany*, 51 Spec No, pp.459–73. Available at: http://www.ncbi.nlm.nih.gov/pubmed/10938854 [Accessed April 9, 2018].

Seitz, S.M. et al., 2006. A Comparison and Evaluation of Multi-View Stereo Reconstruction Algorithms. In *2006 IEEE Computer Society Conference on Computer Vision and Pattern Recognition - Volume 1 (CVPR'06)*. IEEE, pp. 519–528. Available at: http://dl.acm.org/citation.cfm?id=1153170.1153518 [Accessed January 12, 2016].

Seitz, S.M., 2000. A Theory of Shape by Space Carving. *International Journal of Computer Vision*, 38(3), pp.199–218.

Sticklen, M.B., 2007. Feedstock Crop Genetic Engineering for Alcohol Fuels. *Crop Science*, 47(6), p.2238. Available at: https://dl.sciencesocieties.org/publications/cs/abstracts/47/6/2238 [Accessed January 6, 2015].

Vasquez-Gomez, J.I., Sucar, L.E. & Murrieta-Cid, R., 2013. Hierarchical Ray Tracing for Fast Volumetric Next-Best-View Planning. In *2013 International Conference on Computer and Robot Vision*. IEEE, pp. 181–187. Available at: http://ieeexplore.ieee.org/lpdocs/epic03/wrapper.htm?arnumber=6569201 [Accessed March 1, 2016].

Wong, L.M., Dumont, C. & Abidi, M.A., 1999. Next best view system in a 3D object modeling task. In *Proceedings 1999 IEEE International Symposium on Computational Intelligence in Robotics and Automation. CIRA'99 (Cat. No.99EX375)*. IEEE, pp. 306–311. Available at: http://ieeexplore.ieee.org/lpdocs/epic03/wrapper.htm?arnumber=810066 [Accessed February 7, 2016].

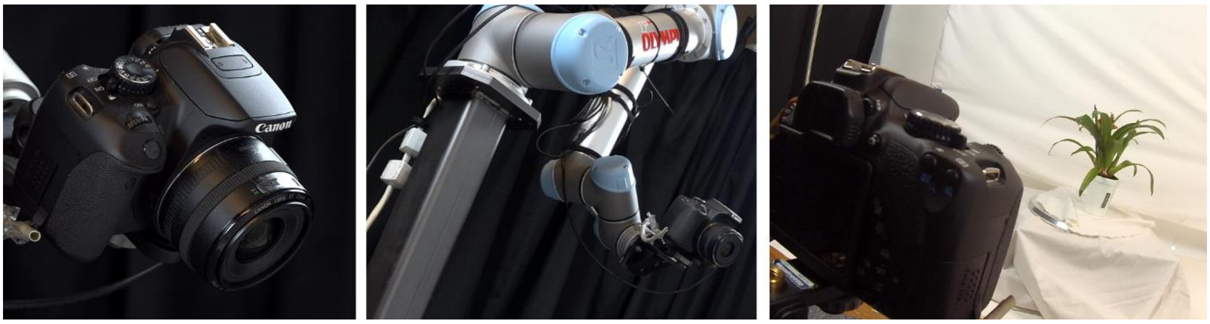


**Figure 1** The Active Vision Cell comprised of a Canon 650D camera, a Universal Robot 5, and an LT360EX turntable upon which the plant is placed

**Figure 2** Initial representation; left an original image of the plant, middle the initial representation after 10 images, right the final voxel model showing more object features after acquiring additional viewpoints

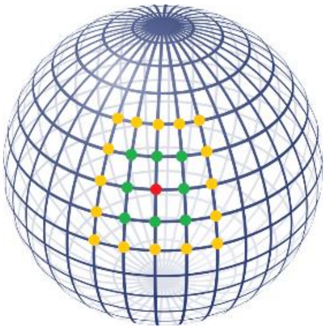

**Figure 3** The view sphere representation which encloses the plant being modelled such that it is centred. The Red dot is an example of an initial *optimal* viewpoint, should this fail it is expanded to green, then to yellow and so on.

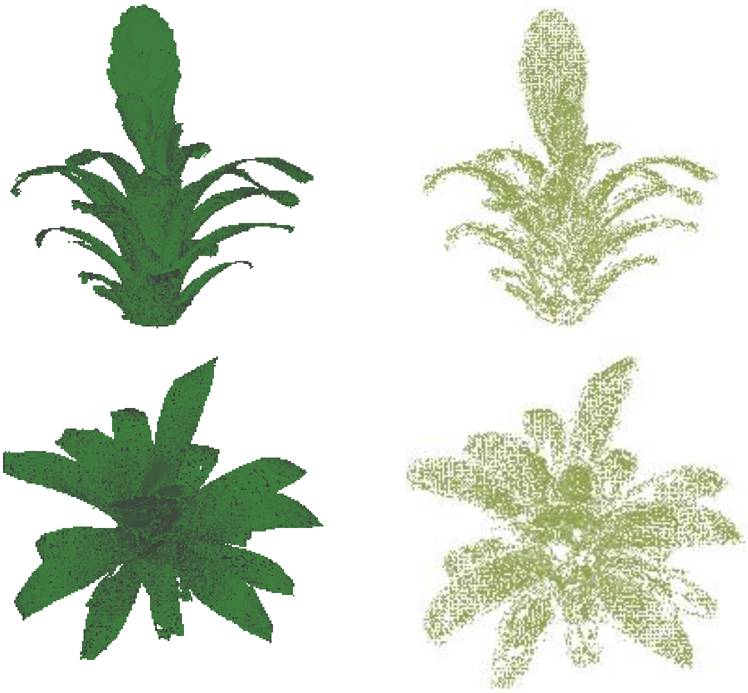

**Figure 4** *Experiment one conducted on a bromeliad (Vriesea sp.). The first column is the X-Ray data, obtained using a CT scanner, the top row presents a side view and the bottom row a top down view. The second column is a point set obtained using the AVC proposed here.*

**Figure 5** *Experiment two conducted on Aloe vera. The first column is the X-Ray data, obtained using a CT scanner, the top row presents a side view and the bottom row a top down view. The second column is a point set obtained using the proposed AVC.*

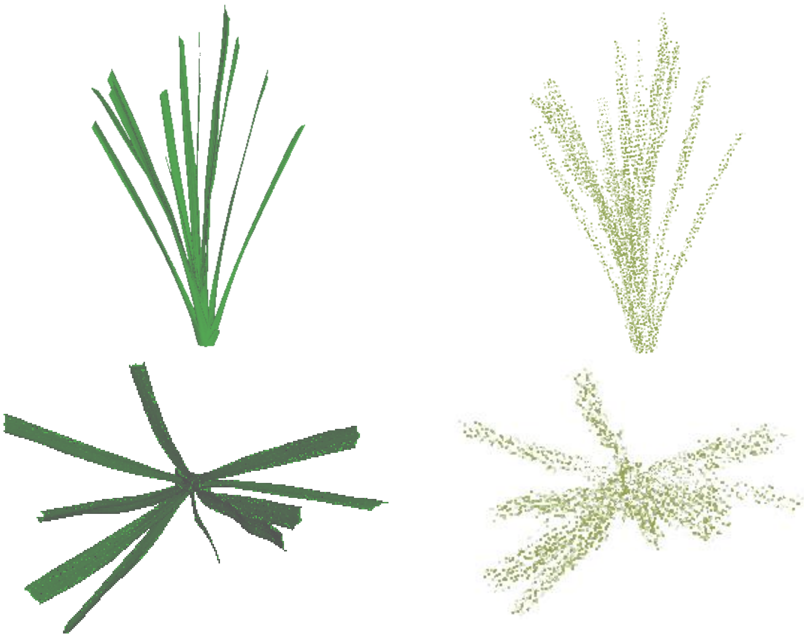

**Figure 6** *Experiment three conducted on a Cordyline (Cordyline sp.). The first column is the X-Ray data, obtained using a CT scanner, the top row presents a side view and the bottom row a top down view. The second column is a point set obtained using the AVC proposed here.*

**Figure 7** *Experiment four conducted on Brassica napus. The first column is the X-Ray data, obtained using a CT scanner, the top row presents a side view and the bottom row a top down view. The second column is a point set obtained using the AVC proposed here.*

**Figure 8** *Experiment five conducted on a chilli plant (Capsicum sp.). The first column is the X-Ray data, obtained using a CT scanner, the top row presents a side view and the bottom row a top down view. The second column is a point set obtained using the AVC proposed here.*

**Figure 9** Experiment six conducted on the Pumpkin (Cucurbita pepo). The first column is the X-Ray data, obtained using a CT scanner, the top row presents a side view and the bottom row a top down view. The second column is a point set obtained using the AVC proposed here.

## Parsed Citations


**Adeloye, A., 2010. Global Warming Impact: Flood Events, Wet-Dry Conditions and Changing Scene in World Food Security. Journal of Agricultural Research and Development, 9(1). Available at: http://www.ajol.info/index.php/jard/article/view/56128 [Accessed January 8, 2015].**
Pubmed: Author and Title
Google Scholar: Author Only Title Only Author and Title

**Aloimonos, J., Weiss, I. & Bandyopadhyay, A., 1988. Active vision. International Journal of Computer Vision, 1(4), pp.333–356. Available at: http://www.scopus.com/inward/record.url?eid=2-s2.0-34250088854&partnerID=tZOtx3y1 [Accessed February 26, 2015].**
Pubmed: Author and Title
Google Scholar: Author Only Title Only Author and Title

**Burgess, A.J. et al., 2017. Exploring Relationships between Canopy Architecture, Light Distribution, and Photosynthesis in Contrasting Rice Genotypes Using 3D Canopy Reconstruction. Frontiers in Plant Science, 8, p.734. Available at: http://journal.frontiersin.org/article/10.3389/fpls.2017.00734/full [Accessed July 26, 2018].**
Pubmed: Author and Title
Google Scholar: Author Only Title Only Author and Title

**Burgess, A.J. et al., 2015. High-Resolution Three-Dimensional Structural Data Quantify the Impact of Photoinhibition on Long-Term Carbon Gain in Wheat Canopies in the Field. Plant Physiology, 169(2), pp.1192–1204. Available at: http://www.ncbi.nlm.nih.gov/pubmed/26282240 [Accessed June 1, 2017].**
Pubmed: Author and Title
Google Scholar: Author Only Title Only Author and Title

**Burgess, A.J. et al., 2016. The 4-Dimensional Plant: Effects of Wind-Induced Canopy Movement on Light Fluctuations and Photosynthesis. Frontiers in plant science, 7, p.1392. Available at: http://www.ncbi.nlm.nih.gov/pubmed/27708654 [Accessed April 9, 2018].**
Pubmed: Author and Title
Google Scholar: Author Only Title Only Author and Title

**Challinor, A. et al., 2014. A meta-analysis of crop yield under climate change and adaptation. Nature Climate Change. Available at: http://eprints.whiterose.ac.uk/78340/13/Challinor-etal-AR5-RevisionsFinal_with_coversheet.pdf [Accessed December 12, 2014].**
Pubmed: Author and Title
Google Scholar: Author Only Title Only Author and Title

**Dornaika, F. & Horaud, R., 1998. Simultaneous robot-world and hand-eye calibration. IEEE Transactions on Robotics and Automation, 14(4), pp.617–622. Available at: http://ieeexplore.ieee.org/lpdocs/epic03/wrapper.htm?arnumber=704233 [Accessed November 27, 2014].**
Pubmed: Author and Title
Google Scholar: Author Only Title Only Author and Title

**Faaij, A., 2008. Bioenergy and global food security, Available at: http://www.wbgu.de/fileadmin/templates/dateien/veroeffentlichungen/hauptgutachten/jg2008/wbgu_jg2008_ex03.pdf [Accessed November 24, 2014].**

**Furbank, R. T., & Tester, M., 2011. Phenomics – technologies to relieve the phenotyping bottleneck. Trends in plant science, 16(12), pp.635–644. Available at: https://www.plantphenomics.org.au/publications/2011TrendsFurbankTester.pdf [Accessed November 1, 2014].**
Pubmed: Author and Title
Google Scholar: Author Only Title Only Author and Title

**Furukawa, Y. & Ponce, J., 2010. Accurate, dense, and robust multiview stereopsis. IEEE transactions on pattern analysis and machine intelligence, 32(8), pp.1362–76. Available at: http://www.ncbi.nlm.nih.gov/pubmed/20558871.**
Pubmed: Author and Title
Google Scholar: Author Only Title Only Author and Title

**Gibbs, J.A. et al., 2017. Approaches to three-dimensional reconstruction of plant shoot topology and geometry. Functional Plant Biology, 44(1), p.62. Available at: http://www.publish.csiro.au/?paper=FP16167 [Accessed November 6, 2017].**
Pubmed: Author and Title
Google Scholar: Author Only Title Only Author and Title

**Hemming, J. et al., 2014. A robot for harvesting sweet-pepper in greenhouses. In Proceedings of the International Conference of Agricultural Engineering. Available at: http://edepot.wur.nl/309949 [Accessed June 16, 2015].**
Pubmed: Author and Title
Google Scholar: Author Only Title Only Author and Title

**Hemming, J. et al., 2014. Fruit detectability analysis for different camera positions in sweet-pepper. Sensors (Basel, Switzerland), 14(4), pp.6032–44. Available at: http://www.mdpi.com/1424-8220/14/4/6032/htm [Accessed June 17, 2015].**
Pubmed: Author and Title
Google Scholar: Author Only Title Only Author and Title

**Hornung, A., Zeng, B., & Kobbelt, L. (2008, June). Image selection for improved multi-view stereo. In Computer Vision and Pattern Recognition, 2008. CVPR 2008. IEEE Conference on (pp. 1-8). IEEE.**
Pubmed: Author and Title

Google Scholar: Author Only Title Only Author and Title

**Long, S.P. et al., 2006. Can improvement in photosynthesis increase crop yields? Plant, cell & environment, 29(3), pp.315–30. Available at: http://www.ncbi.nlm.nih.gov/pubmed/17080588 [Accessed April 9, 2018].**
Pubmed: Author and Title
Google Scholar: Author Only Title Only Author and Title

**Massios, Nikolaos A., and R.B.F., 1998. A best next view selection algorithm incorporating a quality criterion. BMVC.**
Pubmed: Author and Title
Google Scholar: Author Only Title Only Author and Title

**Paproki, A. et al., 2012. A novel mesh processing based technique for 3D plant analysis. BMC plant biology, 12(1), pp.1–13.**
Pubmed: Author and Title
Google Scholar: Author Only Title Only Author and Title

**Poorter, H. et al., 2016. Pampered inside, pestered outside? Differences and similarities between plants growing in controlled conditions and in the field. New Phytologist, 212(4), pp.838–855. Available at: http://www.ncbi.nlm.nih.gov/pubmed/27783423 [Accessed April 9, 2018].**
Pubmed: Author and Title
Google Scholar: Author Only Title Only Author and Title

**Pound, M.P. et al., 2014. Automated recovery of three-dimensional models of plant shoots from multiple color images. Plant physiology, 166(4), pp.1688–98. Available at: http://www.plantphysiol.org/content/166/4/1688 [Accessed December 11, 2014].**
Pubmed: Author and Title
Google Scholar: Author Only Title Only Author and Title

**Quan, L. et al., 2006. Image-based plant modeling. ACM Transactions on Graphics, 25(3), p.599. Available at: http://dl.acm.org/citation.cfm?id=1141911.1141929 [Accessed November 5, 2014].**
Pubmed: Author and Title
Google Scholar: Author Only Title Only Author and Title

**Remondino, F. & El-Hakim, S., 2006. Image-based 3D Modelling: A Review. The Photogrammetric Record, 21(115), pp.269–291. Available at: http://doi.wiley.com/10.1111/j.1477-9730.2006.00383.x [Accessed January 8, 2015].**
Pubmed: Author and Title
Google Scholar: Author Only Title Only Author and Title

**Reynolds, M.P., van Ginkel, M. & Ribaut, J.M., 2000. Avenues for genetic modification of radiation use efficiency in wheat. Journal of experimental botany, 51 Spec No, pp.459–73. Available at: http://www.ncbi.nlm.nih.gov/pubmed/10938854 [Accessed April 9, 2018].**
Pubmed: Author and Title
Google Scholar: Author Only Title Only Author and Title

**Seitz, S.M. et al., 2006. A Comparison and Evaluation of Multi-View Stereo Reconstruction Algorithms. In 2006 IEEE Computer Society Conference on Computer Vision and Pattern Recognition - Volume 1 (CVPR'06). IEEE, pp. 519–528. Available at: http://dl.acm.org/citation.cfm?id=1153170.1153518 [Accessed January 12, 2016].**
Pubmed: Author and Title
Google Scholar: Author Only Title Only Author and Title

**Seitz, S.M., 2000. A Theory of Shape by Space Carving. International Journal of Computer Vision, 38(3), pp.199–218.**
Pubmed: Author and Title
Google Scholar: Author Only Title Only Author and Title

**Sticklen, M.B., 2007. Feedstock Crop Genetic Engineering for Alcohol Fuels. Crop Science, 47(6), p.2238. Available at: https://dl.sciencesocieties.org/publications/cs/abstracts/47/6/2238 [Accessed January 6, 2015].**
Pubmed: Author and Title
Google Scholar: Author Only Title Only Author and Title

**Vasquez-Gomez, J.I., Sucar, L.E. & Murrieta-Cid, R., 2013. Hierarchical Ray Tracing for Fast Volumetric Next-Best-View Planning. In 2013 International Conference on Computer and Robot Vision. IEEE, pp. 181–187. Available at: http://ieeexplore.ieee.org/lpdocs/epic03/wrapper.htm?arnumber=6569201 [Accessed March 1, 2016].**
Pubmed: Author and Title
Google Scholar: Author Only Title Only Author and Title

**Wong, L.M., Dumont, C. & Abidi, M.A., 1999. Next best view system in a 3D object modeling task. In Proceedings 1999 IEEE International Symposium on Computational Intelligence in Robotics and Automation. CIRA'99 (Cat. No.99EX375). IEEE, pp. 306–311. Available at: http://ieeexplore.ieee.org/lpdocs/epic03/wrapper.htm?arnumber=810066 [Accessed February 7, 2016].**
Pubmed: Author and Title
Google Scholar: Author Only Title Only Author and Title